Hindawi
International Journal of Photoenergy
Volume 2020, Article ID 8818136, 7 pages
https://doi.org/10.1155/2020/8818136

Research Article

Study on the Creep Behavior of a Ni_3Al-Based Single Crystal Alloy at 850°C/450 MPa

Liwu Jiang,[1,2] **Yu Yang**,[1] **Meiling Wu**,[3] **and Min Cai**[4]

[1]*National Center for Materials Service Safety, University of Science and Technology Beijing, Beijing 100083, China*
[2]*NCS Testing Technology Co., Ltd., Beijing 100081, China*
[3]*Beijing Institute of Aeronautical Materials, Beijing 100095, China*
[4]*Avic Manufacturing Technology Institute, Beijing 100024, China*

Correspondence should be addressed to Liwu Jiang; lwjiang@ustb.edu.cn

Received 13 August 2020; Revised 21 September 2020; Accepted 22 September 2020; Published 13 October 2020

Academic Editor: Yimin Wu

The creep behaviors of Ni_3Al-based single crystal alloy IC6SX with [001] and [111] orientations under the condition of 850°C/450 MPa were investigated. The effect of crystal orientation on the creep lives, fracture morphology, fracture mechanism, and dislocation evolution of the alloys with different orientations was analyzed systematically. The results showed that the creep lives of the alloy were closely related to the crystal orientation under the condition of 850°C/450 MPa. The creep lives of the single crystal alloys with [001] and [111] orientations were 56.3 h and 126.9 h, respectively. Moreover, the fracture morphologies of the two alloys with [001] and [111] orientations were different. The results showed that some holes formed at the fracture surface of the alloy with [111] rather than [001] orientation. Furthermore, the surface near the fracture of the two alloys with [001] and [111] orientations was serrated. Therefore, the fracture mechanism of the single crystal alloys with [001] and [111] orientations was ductile fracture. In addition, a large number of dislocations cut into the γ' phase. Therefore, the cutting mechanism of dislocations in the alloys with [001] and [111] orientations was the creep deformation mechanism.

1. Introduction

With the development of the turbine vanes of aero-engines, the working temperature and content of precious metals of superalloy turbine blades are increased continuously [1–6]. Ni_3Al-based single crystal alloy has the following advantages, such as low density, strong oxidation resistance, stable structure, and strong creep resistance. Therefore, the alloy has become the most potential material for turbine blades [7–13].

Gui found that the creep resistance of Ni-based single crystal alloy with [111] orientation was better than that with [001] orientation from 1000°C to 1100°C [14]. Other studies showed that the creep resistance and creep rate of Ni-based single crystal alloys with different orientations were different [15–20]. The creep properties of single crystal alloy DD6 were studied by Wang et al. [21]. They pointed that, under the same test condition, the creep life of single crystal alloy DD6 decreased in order of [111], [001] and [011] orientations at 760°C, which was consistent with alloy DD499 under the condition of 1040°C/165 MPa [22]. Su and Tian showed the effect of the crystal orientation on the microstructure of Ni-based single crystal alloy. It was found that the γ' phases of the single crystal alloys with [001], [011] and [111] orientations were transformed into N-type rafted structure, stripe-like rafted structure, and mesh-like rafted structure under 1040°C/137 MPa, respectively [23, 24]. It has also been found that the dendrite morphologies, fracture mechanism, and dislocation evolution of Ni-based single crystal alloys with different orientations were different [25–30]. It is necessary to investigate the creep lives, fracture morphology, and dislocation evolution of the single crystal alloy IC6SX with different crystal orientations.

In this paper, the relationship between creep properties and crystal orientation of Ni_3Al-based single crystal alloy IC6SX at 850°C/450 MPa has been explored. The fracture mechanism, microstructure, and dislocation evolution of

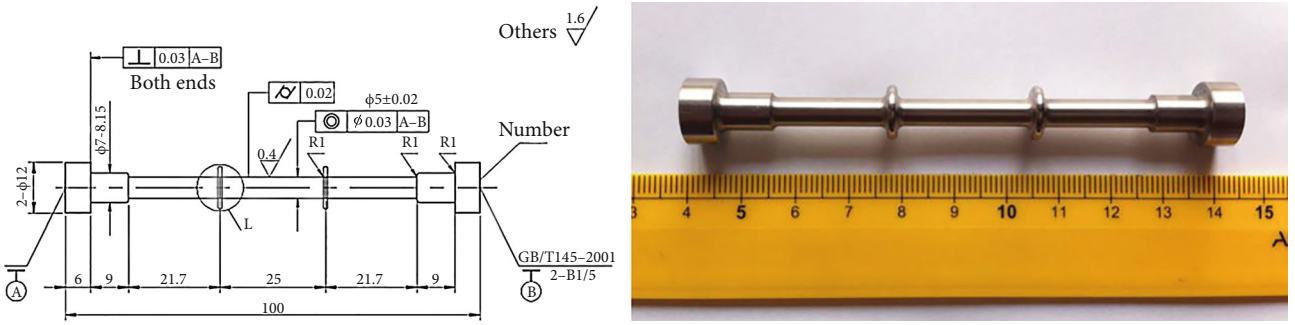

Figure 1: Schematic diagram of processed creep specimen and photo of high-temperature creep specimen.

the Ni_3Al-based single crystal alloys with different orientations were investigated, providing a theoretical basis for the application of Ni_3Al-based single crystal alloy IC6SX.

2. Experimental

The material used for the present study was a Ni_3Al-based single crystal alloy IC6SX, with a nominal composition of Ni-7.4~8.0Al-13.5~14.3Mo-0.02~0.03B (wt%). The single crystal alloy test bars with different crystal orientations were produced by screw selection crystal method in the DZG-0.025 directional solidification furnace. All the test bars were calibrated for crystal orientation by X-ray backscattering Laue method. The bars with orientation deviation less than 10° and without defects were selected for experimental study.

Figure 1 shows that the single crystal alloy was processed into a high-temperature creep specimen after the heat treatment under the condition of 1260°C/10 h + 870°C/32 h. The uniaxial constant load tensile creep tests for the single crystal alloys with [001] and [111] orientations were carried out under the condition of 850°C/450 MPa by the GWT504 high-temperature durable creep testing machine.

The microstructure of creep specimens was analyzed by the ZEISS Axio Imager A2m optical microscope (OM) and ZEISS SUPRA55 scanning electron microscope (SEM). The dislocation morphology of creep specimens was investigated by the Tecnai F30 transmission electron microscope (TEM).

3. Results and Discussion

3.1. Effect of Crystal Orientation on Creep Properties of Single Crystal Alloy. Figure 2 shows the creep curves of the single crystal alloy IC6SX with [001] and [111] orientations at 850°C/450 MPa, and the partial enlarged graph of the region marked by the arrow is shown in the top left corner.

It can be seen from Figure 2 that the creep curves of the single crystal alloy IC6SX were composed of the transient primary creep stage, steady creep stage, and accelerating creep stage. The initial strain of the single crystal alloys with [001] and [111] orientations at 850°C/450 MPa were 0.44% and 0.14%, respectively. The creep lives of the single crystal alloys with [001] and [111] orientations were 56.3 h and 126.9 h, respectively. The minimum steady creep rate of the alloys with [001] and [111] orientations were 1.03×10^{-5} and 1.04×10^{-5}, respectively. The elongation of the alloys

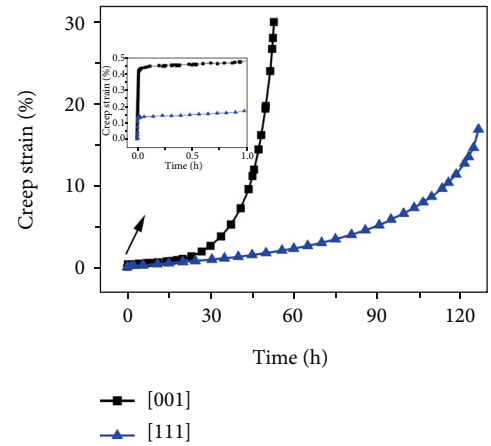

Figure 2: Creep curves of the single crystal alloy IC6SX with [001] and [111] orientations at 850°C/450 MPa.

with [001] and [111] orientations were 31.0% and 19.5%, respectively. Compared with the single crystal alloy with [001] orientation, the creep life of the alloy with [111] orientation was obviously increased, while the elongation was obviously decreased.

3.2. Fracture Morphology and Longitudinal Section Microstructure of Single Crystal Alloys with Different Orientations after Creep Test

3.2.1. Single Crystal Alloy with [001] Orientation. Figure 3 shows the sample photo and the fracture morphology of the single crystal alloy IC6SX with [001] orientation after being crept for 56.3 h and then up to fracture at 850°C/450 MPa.

Figure 3(a) shows that positions A, B, C, and D were the exposed core, transition section B, transition section C, and gauge length of the creep specimen, respectively. As shown in Figure 3(a), in the three positions A, B, and C which were outside the gauge length, there was no obvious deformation. However, a certain degree of the plastic deformation occurred in position D. The surface of the specimen was slightly black and green, which indicated that the surface of the specimen had a slight degree of oxidation in the process of creep. In Figure 3(b), the fracture shape of the specimen changed from circle to ellipse, with the ellipticity (major axis : minor axis) of 1.5. Figure 3(c) is a partial enlarged picture of position A in Figure 3(b), showing a certain number

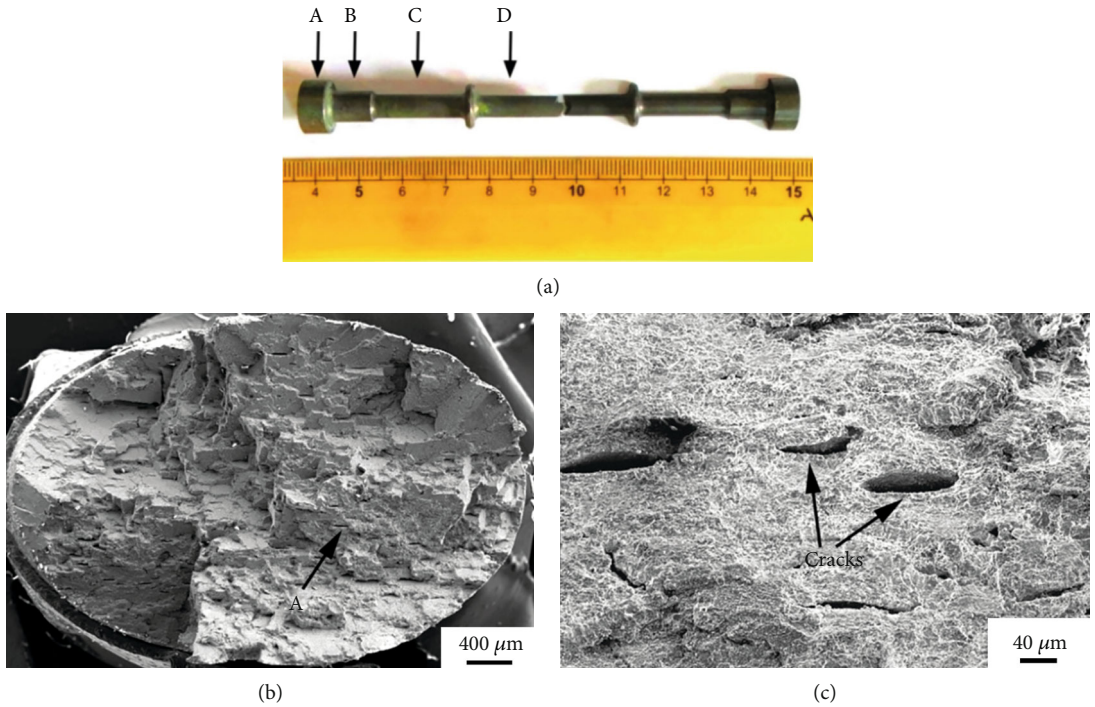

Figure 3: Sample photo and SEM images of the fracture morphology of the single crystal alloy IC6SX with [001] orientation after being crept for 56.3 h and then up to fracture at 850°C/450 MPa. (a) Fracture specimen photo; (b) low multiple fracture morphology; (c) partial enlarged image of position A from (b).

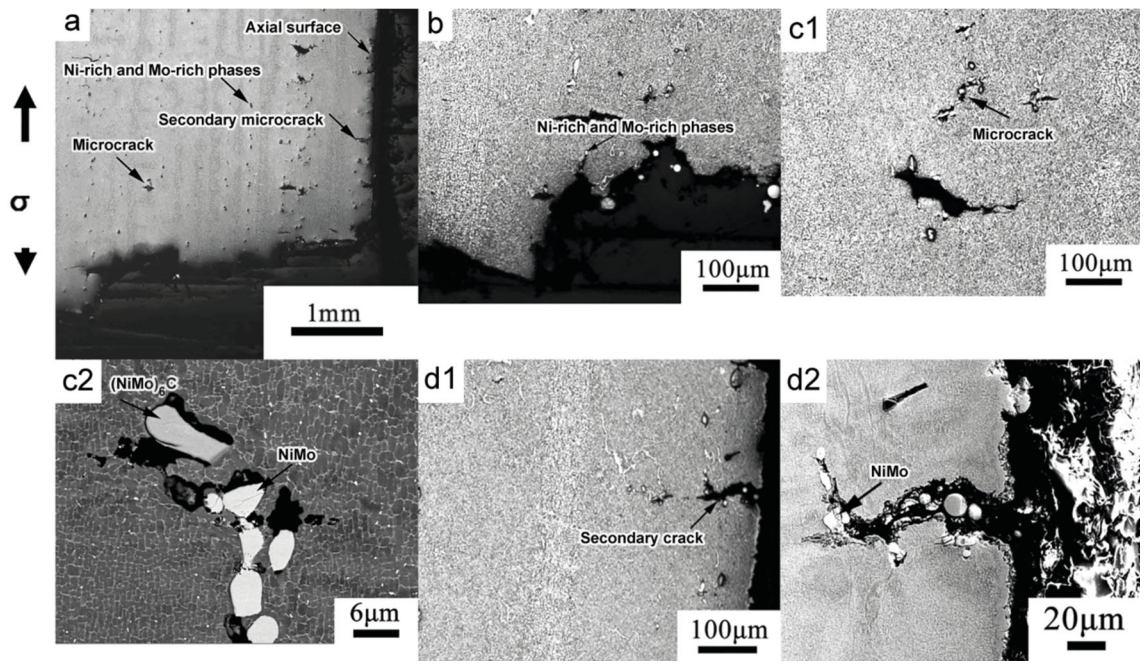

Figure 4: Microstructures of the fracture longitudinal section of the single crystal alloy IC6SX with [001] orientation after being crept for 56.3 h and then up to fracture at 850°C/450 MPa. (a) Macroscopic metallographic structure (OM image); (b) fracture surface cracks (OM image); (c1) microcracks in the interior of the matrix (OM image); (c2) microcracks in the interior of the matrix (SEM image); (d1) secondary crack on the axial surface (OM image); (d2) secondary crack on the axial surface (SEM image).

of cracks on the fracture surface, as shown by the arrow in Figure 3(c).

Figure 4 shows the microstructures of the fracture longitudinal section of the single crystal alloy IC6SX with [001] orientation after being crept for 56.3 h and then up to fracture under the condition of 850°C/450 MPa. It can be seen from Figure 4(a) that creep fracture edge of the single crystal alloy with [001] orientation was approximately

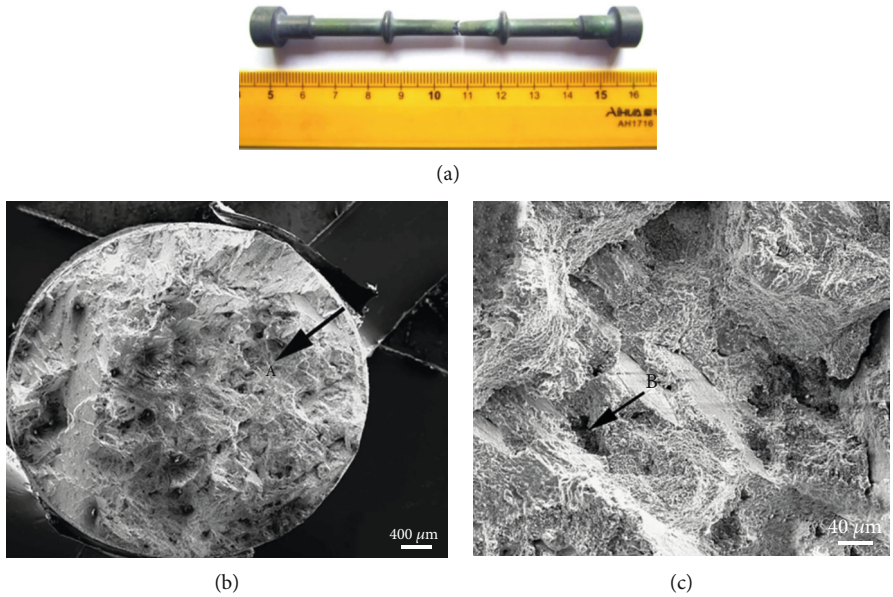

(a)

(b)

(c)

Figure 5: Sample photo and SEM images of fracture morphology of the single crystal alloy IC6SX with [111] orientation after being crept for 126.9 h and then up to fracture at 850°C/450 MPa. (a) Fracture specimen photo; (b) low multiple fracture morphology; (c) partial enlarged image of position A from (b).

perpendicular to the stress axis. The analysis of the macroscopic metallographic structure showed that a large number of microcracks existed at the region near the fracture in the interior of the specimen. In addition, the microcracks, which were distributed along the growth orientation of [001], formed at Ni-rich and Mo-rich phases in the interdendrite region. With the increase of the distance to the fracture surface, the number and size of microcracks decreased gradually. Furthermore, there were a certain number of secondary cracks on the axial surface, and the length of the secondary cracks decreased gradually from the surface near the fracture to the interior of the specimen. Moreover, the directions of microcracks and secondary cracks were perpendicular to the stress axis. From Figure 4(b), it was found that the surface near the fracture was serrated, showing ductile fracture, and the surface cracks near the fracture propagated along the Ni-rich and Mo-rich phases from the fracture to the interior of the alloy. Figures 4(c1) and 4(c2), respectively, show the optical image and SEM image of microcracks within the matrix near the fracture. In addition, Figure 4(c1) indicates that microcracks formed in the interior of the alloy near the fracture. These microcracks generated, connected, and grew at the interface between the Ni-rich, Mo-rich and the matrix, as shown in Figure 4(c2). Figures 4(d1) and 4(d2) show the optical image and SEM image of the surface secondary crack near the fracture, respectively. It can be seen from Figure 4(d1) that under the action of tensile stress the secondary cracks along the axial surface were perpendicular to the stress axial and propagated to the interior of the specimen. Due to the existence of Ni-rich and Mo-rich phases near the axial surface in the alloy, the direction of the secondary cracks changed. Moreover, the secondary cracks connected with the microcracks around the Ni-rich and Mo-rich phases, as shown in Figure 4(d2).

3.2.2. Single Crystal Alloy with [111] Orientation. Figure 5 shows the sample photo and the fracture morphology of the single crystal alloy IC6SX with [111] orientation after being crept for 126.9 h and then up to fracture at 850°C/450 MPa.

It can be seen from Figure 5(b) that the fracture shape of the specimen was approximately circle, and the enlarged photo of position A is shown in Figure 5(c). Figure 5(c) indicates that there were some holes in the fracture surface, as shown by arrow B in Figure 5(c).

Figure 6 indicates the microstructures of fracture longitudinal section of the single crystal alloy IC6SX with [111] orientation after being crept for 126.9 h and then up to fracture at 850°C/450 MPa. It can be seen from Figure 6(a) that the angle between the creep fracture edge of the alloy and the stress axis was about 45°. The analysis of the macroscopic metallographic structure showed that within the specimen a certain number of microcracks existed at the region near the fracture. In addition, the microcracks formed in the interdendritic region of the Ni-rich and Mo-rich phases and were distributed diffusely. The number and the size of microcracks decreased gradually from the fracture surface to the interior of the specimen. There was a certain angle between the direction of the microcracks and the stress axis. A few secondary cracks with the small length existed on the axial surface. Figure 6(b) is the enlarged picture of region A in Figure 6(a). Figure 6(b) indicates that the surface near the fracture was serrated, which was a ductile fracture. In addition, the surface crack near the fracture propagated to the interior of the specimen along the Ni-rich, Mo-rich phases and dendritic arm. Figures 6(c1) and 6(c2) show the optical image and SEM image of internal microcracks within the matrix near the fracture surface, respectively. In addition, Figure 6(c1) indicates that a few microcracks formed in the alloy near the fracture, and Figure 6(c2) shows that the cracks generated, connected, and grew at the interface between the

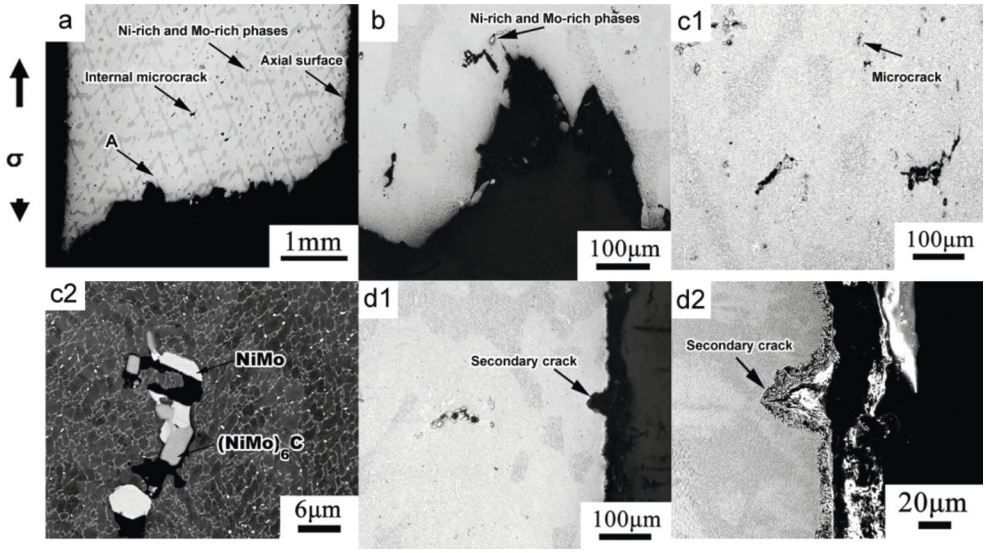

Figure 6: Microstructures of fracture longitudinal section of the single crystal alloy IC6SX with [111] orientation after being crept for 126.9 h and then up to fracture at 850°C/450 MPa. (a) Macroscopic metallographic structure (OM image); (b) fracture surface cracks (OM image); (c1) microcracks in the interior of the matrix (OM image); (c2) microcracks in the interior of the matrix (SEM image); (d1) secondary crack on the axial surface (OM image); (d2) secondary crack on the axial surface (SEM image).

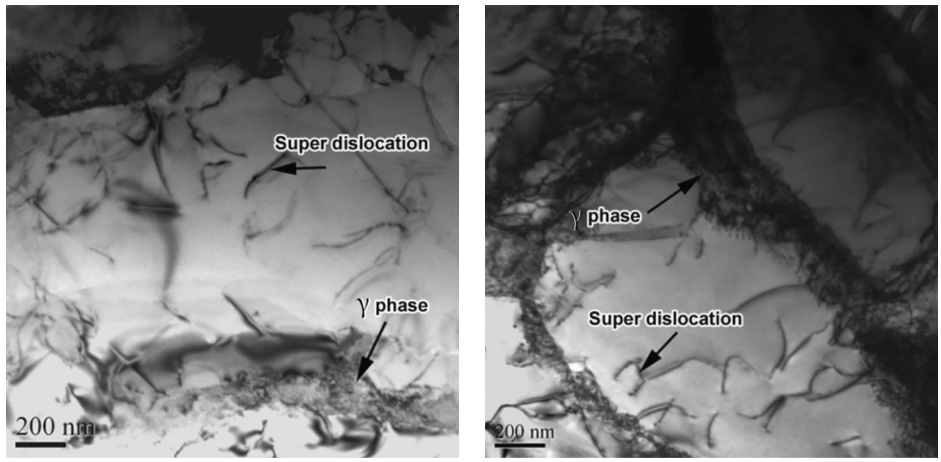

(a) (b)

Figure 7: Dislocation configuration of the single crystal alloy with different orientations after creep rupture at 850°C/450 MPa: (a) [001] orientation; (b) [111] orientation.

Ni-rich, Mo-rich phases and the matrix. Figures 6(d1) and 6(d2) show the optical image and SEM image of the surface secondary cracks near the fracture, respectively. Moreover, Figure 6(d1) indicates that under the action of tensile stress, there were secondary cracks along the surface. It can be seen from Figure 6(d2) that the crack propagated along the direction perpendicular to the stress axial to the interior of the specimen, and the crack tip was obviously oxidized, causing passivation of the crack tip.

3.3. Evolution of Dislocations during Creep of Single Crystal Alloys with Different Crystal Orientations. Figure 7 shows the dislocation configuration of the single crystal alloys with [001] and [111] orientations after creep rupture at 850°C/450 MPa. It can be seen that the dislocation configuration of the single crystal alloy with [001] orientation was similar to that with [111] orientation after creep fracture. In addition, a large number of dislocations generated in the γ channels, cutting into the γ' phase. Consequently, the cutting mechanism of dislocations in the alloys with [001] and [111] orientations under high stress was the main creep deformation mechanism.

3.4. Analysis and Discussion. Due to the low temperature and high stress, the dislocations move in slip mode. However, in addition to the relative displacement of the slip plane, the single crystal slip is often accompanied by the rotation of the crystal planes, leading to the elliptical deformation of the alloy. Owing to primary NiMo phase and $(NiMo)_6C$ phase

with incomplete solid solution which are both the hard brittle phase existed within the single crystal alloys with different orientations, the dislocations will pile up and result in stress concentration when reaching the hard brittle phase. When the stress concentration reaches a certain level, the cracks form in and around the primary NiMo phase and $(NiMo)_6C$ phase. Moreover, under the action of the tensile stress, the cracks connect with each other and extend to the interior of the specimen.

Therefore, within the gauge length, due to the large deformation of the specimen, a large number of dislocations pile up at the interdendritic interface between the primary NiMo phase and matrix phase or between the $(NiMo)_6C$ phase and matrix phase near the fracture, causing the crack formation around the interface. In addition, the elongation direction of the cracks is approximately perpendicular to the stress axis. However, the cracks hardly form in the gauge length away from the fracture. At the same time, a certain number of secondary cracks are also found on the surface near the fracture of the specimen, and there are hard and brittle phases at the crack tip. Due to the high temperature during creep, the surface of the specimen is easy to oxidize. Under the action of the tensile stress, dislocations are easy to pile up near the hard and brittle oxides, resulting in stress concentration. When the stress concentration reaches a certain level, the microcracks form and further propagate to the interior of the specimen in the direction perpendicular to the tensile stress. When extending to a certain extent, the cracks meet with the microcracks which were formed around the hard and brittle phases between dendrites, which accelerate the microcrack propagation, further leading to the fracture of the specimen.

Because the fracture shape of the alloy with [001] orientation changes from circle to ellipse, the deformation degree of the alloy with [001] orientation is larger than that of the alloy with [111] orientation within the gauge length. A certain number of cracks of the two alloys with [001] and [111] orientations form at the interface between the primary NiMo phase or $(NiMo)_6C$ phase and the matrix phase near the fracture. However, the total number of cracks of the alloy with [001] orientation is obviously larger than that of the alloy with [111] orientation. Therefore, the creep life of the alloy with [001] orientation is shorter than that of the alloy with [111] orientation. In addition, it is found that the surfaces near the fracture of the [001] and [111] orientations are serrated. Therefore, the fracture mechanisms of the two alloys are ductile fracture.

4. Conclusion

(1) The creep life of the single crystal alloy IC6SX with [111] orientation is longer than that of the alloy with [001] orientation. In addition, the cracks form at the interdendritic interface between the primary NiMo phase and the matrix or between the $(NiMo)_6C$ phase and the matrix phase near the fracture, with the elongation direction of the cracks approximately perpendicular to the stress axis

(2) Under the condition of 850°C/450 MPa, the fracture morphology of the single crystal alloy with [001] orientation is ellipse, while that with [111] orientation is circle. The fracture mechanisms of the two alloys with [001] and [111] orientations are ductile fracture

(3) Under the condition of 850°C/450 MPa, the creep deformation mechanism of dislocations is mainly dislocation cutting mechanism in the alloys with [001] and [111] orientations

Data Availability

The research data used to support the findings of this study are included within the article.

Conflicts of Interest

No conflict of interest exists in the submission of this manuscript.

Acknowledgments

This research was supported by the National Science and Technology Major Project (Grant No. 2017-VI-0012-0084, 2017-VI-0011-0083), the Fundamental Research Funds for the Central Universities (Grant No. FRF-GF-19-029B) and the National Natural Science Foundation of China (Grant No. 51471022).

References

[1] J. Zhang, L. Wang, D. Wang et al., "Recent progress in research and development of nickel-based single crystal superalloys," *Acta Metallurgica Sinica*, vol. 55, no. 9, p. 1077, 2019.

[2] G. Liu, L. Liu, Z. H. Han, G. J. Zhang, and J. Zhang, "Solidification behavior of Re-and Ru-containing Ni-based single-crystal superalloys with thermal and metallographic analysis," *Rare Metals*, vol. 36, no. 10, p. 792, 2016.

[3] R. C. Reed, T. Tao, and N. Warnken, "Alloys-by-design: application to nickel-based single crystal superalloys," *Acta Materialia*, vol. 57, no. 19, pp. 5898–5913, 2009.

[4] J. Y. Chen, L. M. Cao, M. Xue, and L. J. Liu, "Microstructure and stress rupture property of an experimental single crystal Ni-base superalloy with different heat treatments," *Rare Metals*, vol. 33, no. 2, pp. 144–148, 2014.

[5] K. D. Xu, Z. M. Ren, and C. J. Li, "Progress in application of rare metals in superalloys," *Rare Metals*, vol. 33, no. 2, pp. 111–126, 2014.

[6] W. Y. Ma, Y. F. Han, S. S. Li, Y. R. Zheng, and S. K. Gong, "Effect of Mo content on the microstructure and stress rupture of a Ni-based single crystal superalloy," *Acta Metallurgica Sinica*, vol. 42, no. 11, p. 1191, 2006.

[7] Z. G. Kong and S. S. Li, "Effects of temperature and stress on the creep behavior of a Ni_3Al base single crystal alloy," *Progress in Natural Science: Materials International*, vol. 23, no. 2, pp. 205–210, 2013.

[8] Y. F. Han, "Development of Ni_3AI and its alloys," *Journal of Aeronautical Materials*, vol. 10, no. 1, p. 53, 1990.

[9] Q. Gao, Y. D. Gong, and Y. G. Zhou, "Experimental study on surface roughness in micro-milling of single crystal Ni_3AI-

based superalloy," *China Mechanical Engineering*, vol. 27, no. 6, p. 801, 2016.

[10] R. Q. Wang, B. Zhang, and D. Y. Hu, "Creep constitutive model of Ni_3Al-based single crystal superalloy," *Journal of Aerospace Power*, vol. 33, no. 3, p. 657, 2018.

[11] Y. X. Wu, H. Zhang, F. L. Li, S. S. Li, S. K. Gong, and Y. F. Han, "Kinetics and microstructural evolution during recrystallization of a Ni_3Al-based single crystal superalloy," *Transactions of Nonferrous Metals Society of China*, vol. 22, no. 9, pp. 2098–2105, 2012.

[12] L. W. Jiang, S. S. Li, Z. C. Qiu, and Y. F. Han, "Effects of withdrawal rate on microstructure and stress rupture properties of a Ni_3Al-based single crystal superalloy IC6SX," *Acta Metallurgica Sinica*, vol. 45, no. 5, p. 547, 2009.

[13] J. Yang, W. Kao, and C. Liu, "Development of nickel aluminide matrix composites," *Materials Science and Engineering A*, vol. 107, pp. 81–91, 1989.

[14] Z. L. Gui, "Status of the study on anisotropy of single crystal superalloys in Russia," *Aviation Maintenance and Engineering*, vol. 1, p. 20, 1997.

[15] F. Latief, K. Kakehi, and H. Murakami, "Anisotropic creep behavior of aluminized Ni-based single crystal superalloy TMS-75," *Materials Science and Engineering A*, vol. 567, pp. 65–71, 2013.

[16] V. Sass and M. Feller-Kniepmeier, "Orientation dependence of dislocation structures and deformation mechanisms in creep deformed CMSX-4 single crystals," *Materials Science and Engineering A*, vol. 245, no. 1, pp. 19–28, 1998.

[17] P. Lukas, J. Cadek, V. Sustek, and L. Kunz, "Creep of CMSX-4 single crystals of different orientations in tension and compression," *Materials Science and Engineering A*, vol. 208, no. 2, pp. 149–157, 1996.

[18] V. Sass, U. Glatzel, and M. Feller-Kniepmeier, "Anisotropic creep properties of the nickel-base superalloy CMSX-4," *Acta Materialia*, vol. 44, no. 5, pp. 1967–1977, 1996.

[19] P. Nörtershäuser, J. Frenzel, A. Ludwig, K. Neuking, and G. Eggeler, "The effect of cast microstructure and crystallography on rafting, dislocation plasticity and creep anisotropy of single crystal Ni-base superalloys," *Materials Science & Engineering A*, vol. 626, pp. 305–312, 2015.

[20] P. Y. Wei, Z. G. Yang, X. M. Cheng, Z. G. Zhong, C. Li, and S. Z. Liu, "Tensile creep anisotropy of single crystal superalloy DD3," *Journal of Aeronautical Materials*, vol. 19, no. 3, p. 7, 1999.

[21] K. G. Wang, J. R. Li, S. Z. Liu, Y. Li, and C. X. Cao, "Study on creep properties of DD6 single crystal superalloy at 760°C," *Journal of Materials Engineering*, vol. 5, p. 7, 2004.

[22] G. M. Han, J. J. Yu, X. F. Sun, H. R. Guan, and Z. Q. Hu, "Anisotropic stress rupture behavior of a nickel-based single crystal superalloy," *Rare Metal Materials and Engineering*, vol. 4, p. 673, 2011.

[23] Y. Su, S. G. Tian, H. C. Yu, D. L. Shu, and S. Liang, "Microstructure evolution and its effect on creep behavior of single crystal Ni-based superalloys with various orientations," *Materials Science and Engineering A*, vol. 668, p. 243, 2016.

[24] S. G. Tian, Y. Su, H. C. Yu, and D. L. Shu, "Microstructure evolution and creep properties of a single crystal nickel-based superalloy with various orientations," *Materials Science Forum*, vol. 4074, no. 1758, p. 1951, 2017.

[25] C. B. Yang, L. Liu, X. B. Zhao, Y. F. Li, J. Zhang, and H. Z. Fu, "Dendrite morphology and evolution mechanism of nickel-based single crystal superalloys grown along the <001> and <011> orientations," *Progress in Natural Science: Materials International*, vol. 22, no. 5, pp. 407–413, 2012.

[26] J. L. Liu, T. Jin, J. H. Zhang, and Z. Q. Hu, "Influence of crystal orientation on microstructure and segregation of Ni base single crystal superalloy," *The Chinese Journal of Nonferrous Metals*, vol. 12, no. 4, p. 764, 2002.

[27] C. B. Yang, L. Liu, X. B. Zhao, G. Liu, J. Zhang, and H. Z. Fu, "Dendrite arm spacings and microsegregations in (001) and (011) orientated single crystal superalloys DD407," *Acta Metallurgica Sinica*, vol. 47, no. 10, p. 1246, 2011.

[28] X. B. Zhao, S. F. Gao, C. B. Yang et al., "Influence of crystal orientation on microstructure and mechanical properties and its control for nickel-base single crystal superalloys," *Rare Metals Letters*, vol. 32, no. 1, p. 24, 2013.

[29] S. G. Tian, L. L. Yu, S. Zhang, H. C. Yu, B. J. Qian, and L. Xiao, "Influence of crystal orientations on creep behaviors of single crystal nickel-based superalloy," *The Chinese Journal of Nonferrous Metals*, vol. 21, no. 2, p. 356, 2011.

[30] Z. K. Zhang, B. Z. Wang, D. S. Liu, Z. X. Wen, and Z. F. Yue, "Creep properties and fracture mechanism of DD6," *Journal of Materials Science and Engineering*, vol. 30, no. 3, p. 375, 2012.